Eastern Section

Anomalous Crustal Stress in the Eastern Tennessee Seismic Zone

Will Levandowski*[1], Christine Powell[2], Martin Chapman[3], and Qimin Wu[4]

Abstract

The eastern Tennessee seismic zone (ETSZ) experiences the second highest rates of natural seismicity in the central and eastern United States (CEUS), following the New Madrid area, yet the cause of elevated earthquake rates is unknown. We probe the origin of ETSZ seismicity using geomechanically constrained stress inversions of earthquake focal mechanisms from 57 earthquakes, including 24 newly derived here and five from the recent events not used in the previous stress studies. Highly oblique northwest–southeast (NW–SE) extension that is unique in the CEUS dominates the ETSZ—central Alabama to southeastern Kentucky—and preferentially reactivates normal to strike-slip faults in the northeast (NE) and southwest (SW) quadrants (strikes 018°–086° or 196°–272° and dips 55°–90°). This extension cannot be explained by the compressive tectonic plate-boundary tractions that cause oblique NE–SW contraction elsewhere in the CEUS. Although our analyses do not uniquely determine the origin of the anomalous stress, we favor isostatic disequilibrium, due to anything from surface processes to crust–mantle interactions, as the possible cause. Increased long-term seismic hazard in the ETSZ may be controlled by and confined to the spatial extent of this anomalous seismotectonic state.

Cite this article as Levandowski, W., C. Powell, M. Chapman, and Q. Wu (2023). Anomalous Crustal Stress in the Eastern Tennessee Seismic Zone, *Seismol. Res. Lett.* **XX**, 1–13, doi: 10.1785/0220220364.

Supplemental Material

Introduction

Earthquake rates are roughly ten times higher in the eastern Tennessee seismic zone (ETSZ) than the central and eastern United States (CEUS) average, second only to the New Madrid region (e.g., Petersen *et al.*, 2014). With 2.4 $M_L \geq 3$ earthquakes per year and a Gutenberg–Richter *b*-value of ~0.94 (Bockholt *et al.*, 2015), an M_L 6 event is anticipated every ~275 yr; but, in contrast to New Madrid, no large historical shock is known.

Globally proposed explanations for locally elevated seismicity rates in intraplate settings like the ETSZ can be grouped into four categories. It has been suggested that intraplate aftershock sequences may persist for 1000 yr or more (Stein and Liu, 2009), so the simplest scenario is that concentrations of modern earthquakes are principally the legacy of a major but unknown prehistoric event rather than the result of locally elevated long-term strain accrual (e.g., Ebel *et al.*, 2000). Nevertheless, epidemic-type aftershock sequence models demonstrate that only ~0.04 of the 2.4 annual $M_L \geq 3$ ETSZ earthquakes (0.21 per year or less at 95% confidence) could be ascribed to aftershocks of a large earthquake that occurred on the eve of European colonization (Levandowski and Powell, 2018).

In contrast to aftershocks, earthquakes in the three remaining situations chiefly release long-term strain, yet they have different implications for long-term seismic hazard. Intraplate seismicity often clusters in space and time (e.g., Clark *et al.*, 2012). Therefore, ETSZ events could represent a naturally active phase of strain release in what is a broadly uniform long-term stress and thus strain-rate field (here, "stress" refers to the deviatoric component of the tensor sum of forces responsible for fault loading, or strain accrual). If so, seismic hazard needs not be stationary, and damaging earthquakes may be equally likely in and outside of the ETSZ (e.g., Stein and Liu, 2009). The third class of explanations invokes weakness, such as through low-viscosity ductile lithosphere, low-friction brittle faults, or characteristically low stress-drop events. Under uniform loading, weak areas may experience higher strain rates, higher earthquake rates, or both. In this case, future seismicity rates would remain higher in the ETSZ than elsewhere in the CEUS, and past events may outline the most likely locations of future impactful earthquakes. Finally, stress could be distinct in seismically active regions: localized sources of stress sum in a tensor sense with regional stress, perturbing the net stress state and potentially resulting in a higher magnitude deviatoric stress tensor and thus

1. Tetra Tech, Inc., Chapel Hill, North Carolina, U.S.A., https://orcid.org/0000-0003-4903-5012 (WL); 2. CERI, University of Memphis, Memphis, Tennessee, U.S.A.; 3. Department of Geosciences, Virginia Tech, Blacksburg, Virginia, U.S.A., https://orcid.org/0000-0003-2956-8305 (MC); 4. Lettis Consultants International, Inc., Concord, California, U.S.A., https://orcid.org/0000-0001-8315-8388 (QW)

*Corresponding author: Will.Levandowski@tetratech.com

greater fault loading rates. As in weak zones, seismic hazard would again be roughly stationary over time.

The crustal stress field may shed light on the seismotectonics of the ETSZ and in so doing help to differentiate among these three remaining possibilities. Naturally periodic strain release should reflect the long-term stress field, so the ETSZ stress field would be indistinguishable from its surroundings. Similarly, weak material would strain faster in a uniform stress field; but the rheology of a material does not control the stress applied to it, although stress axis rotations along rheologic boundaries (e.g., Ravat, 1987) such as the New York–Alabama Lineament (NYAL) or other crustal to lithospheric scale contrasts are possible. A significantly different and consistent state of stress across the ETSZ could not readily be explained by weak material or temporal clustering, however, and would instead suggest a localized source of stress.

Although ETAS modeling indicates that postseismic perturbations related to prehistoric earthquakes alone do not explain modern earthquake rates (Levandowski and Powell, 2018), they cannot be entirely ruled out as a source of stress variations in or across the ETSZ. Tectonic loading (i.e., "stress", as used herein) rates in the CEUS are low to immeasurable (e.g., Calais *et al.*, 2010), so the impacts of postseismic perturbations related to prehistoric earthquakes could be comparatively long lived (e.g., Ebel, 2008). The magnitude of this superposed stress may be small, considering as an upper bound that coseismic stress drops in the eastern U.S. average a few MPa (Boyd *et al.*, 2017), compared to the ∼200 MPa differential stress required for frictional slip at seismogenic depths (e.g., Townend and Zoback, 2001), and the impacts may be restricted to areas along the mainshock faults. For instance, following the 2002 **M** 7.9 Denali, Alaska, earthquake, aftershocks along the fault within ∼10 km either side of the rupture revealed clockwise $\sigma_{H\max}$ rotations between 8° ± 22° and 33° ± 39° (2 std), whereas changes in the style of faulting (i.e., the parameter $A\Phi$, discussed subsequently) were minor and moreover varied along the rupture, encouraging more strike slip in some places and more reverse faulting in others (Wesson and Boyd, 2007). Similarly, focal mechanisms from postmainshock seismicity within ∼5 km of the 2011 M 5.8 Mineral, Virginia, and 1886 M ∼7 Charleston, South Carolina, epicenters display vaguely radial $\sigma_{H\max}$ orientations about the mainshock (Levandowski, Herrmann, *et al.*, 2018), again with no significant deviations in faulting style. Based on these analogies, an influence from prehistoric seismicity could manifest as short-wavelength $\sigma_{H\max}$ anomalies along the causative structure, but we contend that the magnitude of any remnant perturbations ought to be small relative to in situ differential stress at seismogenic depths.

A distinct net stress state in the ETSZ that results from the superposition of a localized source of stress, regardless of its origin, with the regional stress field would not necessarily explain elevated seismicity rates. If the magnitude of the deviatoric component of the summed tensor is smaller than the regional deviatoric stress, then lower strain and earthquake rates would be expected, and another cause of the focused seismicity would need to be invoked. By contrast, a secondary stress could explain elevated earthquake rates in the ETSZ if the magnitude of the deviatoric component of the summed regional stress plus local perturbation exceeds the magnitude of that regional stress.

We compile and invert focal mechanisms from 57 ETSZ earthquakes to determine the state of stress and allow quantitative comparison with focal mechanisms from surrounding areas. This comparison maps the extent of the ETSZ stress field and sheds light on the seismotectonic underpinnings of focused seismicity in the ETSZ.

Geologic and Geophysical Setting

The ETSZ is defined by an ∼250 km north-northeast (NNE)–south-southwest (SSW) band of seismicity that parallels the grain of the southern Appalachians (Fig. 1a,b). Nevertheless, hypocenters are not associated with Paleozoic faults or overthrust units, but occur within Grenville-age basement (e.g., Powell *et al.*, 2014). Unlike many other intraplate seismic zones (e.g., Johnston and Kanter, 1990), including New Madrid, the ETSZ is not associated with rifted lithosphere. The area of most concentrated seismicity is, however, tightly bounded along its northwest by a major Proterozoic strike-slip boundary (Steltenpohl *et al.*, 2010; Powell and Thomas, 2016). This basement feature manifests as the NYAL—a 1600 km long magnetic anomaly (King and Zietz, 1978). Seismicity mainly occurs in comparatively nonmagnetic basement southeast (SE) of the shear (Fig. 1a), within a negative Bouguer and isostatic residual gravity anomaly (Fig. 1b).

Shear along the NYAL demonstrably strained adjacent crust and mantle lithosphere, but this ancient deformation is not a sufficient condition for modern seismicity: The ETSZ is the only location along the NYAL that is anomalously seismogenic. Strain in the mantle lithosphere manifests in NYAL-parallel SKS fast directions (Wagner *et al.*, 2012; Long *et al.*, 2016), both within the ETSZ and elsewhere along strike. Crustal modification is suggested by low group-velocity crust (to at least 15 s period) in the ETSZ that is flanked by higher velocity regions (Bockholt, 2015; Brandmayr *et al.*, 2016) and by deeper magnetic basement along the NYAL (6–12 km) than its surroundings (0–4 km) (Brandmayr and Vlahovic, 2016). As with northeast–southwest (NE–SW) fast directions, however, deep magnetic basement and surface-wave anomalies continue NE and SW along strike beyond the epicentral region into seismically quiescent areas. The lack of earthquakes elsewhere implies that the presence and activity of the lithospheric scale shear zone is insufficient to explain earthquake localization in the ETSZ. In addition, geophysical evidence does not support upper mantle thinning, warming, or weakening along the NYAL: both teleseismic *P*-wave tomography (Biryol *et al.*, 2016) and long-period surface-wave dispersion (Pollitz and Mooney, 2016; Shen and

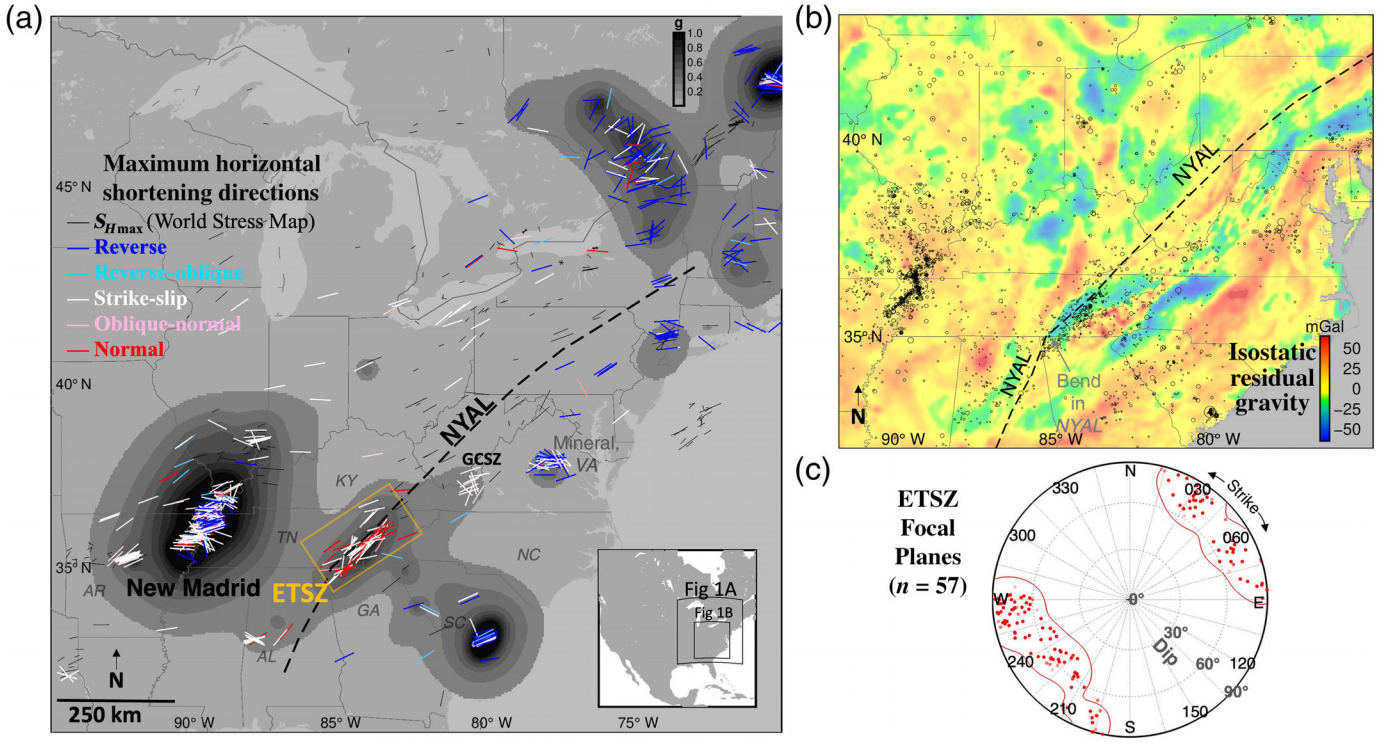

Figure 1. (a) Overview. Focal mechanism *SH* max (colored by faulting style; orientations smoothed over 5 km for clarity). Black bars: World Stress Map indicators (lengths scale with quality). Background shading: Seismic hazard (2 Hz Peak ground acceleration as a fraction of *g* with 2% probability of exceedance in 50 yr, or 2475 yr return period). AL, Alabama; ETSZ, Eastern Tennessee Seismic Zone; GA, Georgia; GCSZ, Giles County Seismic Zone, Virginia; KY, Kentucky; NC, North Carolina; NYAL, New York–Alabama geophysical lineament (after Brandmayr *et al.*, 2016); SC, South Carolina; TN, Tennessee; VA, Virginia. Inset shows locations with respect to eastern North America. (b) Isostatic residual gravity. The ETSZ occupies a negative gravity anomaly centered on the NYAL that is unlike the modest positive anomalies elsewhere along the NYAL. (c) ETSZ fault orientations. Polar plot of geomechanically favorable focal planes from 57 ETSZ focal mechanisms. Orientations are confined to strike/dip ranges 013°–092°/65°–90° and 195°–275°/50°–90°. The color version of this figure is available only in the electronic edition.

Ritzwoller, 2016; Wagner *et al.*, 2012) image higher velocity upper mantle beneath the ETSZ than the adjacent and largely aseismic Piedmont and Triassic basins, and ETSZ heat flow is modestly low relative to surroundings (~35 versus ~45 mW/m^2; Blackwell *et al.*, 2011). Finally, modern earthquakes do not occur on the major NE–SW-trending shear, but rather on high-angle east (E)–west (W)-striking or NNE–SSW-striking faults (Chapman *et al.*, 1997) and on ~60°-dipping NE–SW planes (Fig. 1c). These observations challenge a direct, causal link between the Proterozoic boundary and modern seismicity.

Nevertheless, the ETSZ is associated with spatially limited crustal structure that may play an important role in the localization of earthquake activity. The NYAL bends southward in the southern part of the ETSZ, near the Tennessee-Georgia border (Fig. 1a,b): A set of brittle relay structures would have been necessary to accommodate this bend in the Proterozoic shear system, creating a zone of "concentrated crustal deformation" (Thomas and Powell, 2017) and right-stepping fault sets at the modern ETSZ. Sinistral NYAL motion documented in apparent polar wander curves (D'Agrella-Filho *et al.*, 2008) implies that these secondary faults initiated as high-angle releasing structures. There, local earthquake tomography images a near-vertical low-V_P and low-V_S zones to at least 24 km depth; jointly considering absolute velocities, gravity, and magnetic signatures, Powell *et al.* (2014) suggest mylonitized crust in this heavily deformed relay zone. Anomalously high lower crustal electrical conductivity is also documented in this area (Murphy and Egbert, 2017; Murphy *et al.*, 2019). In addition, the Moho in the southern ETSZ, near the bend in the NYAL, appears gradational or is absent on receiver functions, which has been interpreted to reflect lower crustal delamination, serpentinization, or other localized modification (Graw *et al.*, 2015). Whereas the NYAL as a whole cannot be directly related to focused ETSZ seismicity, these spatially limited crustal features related to large-scale Proterozoic shear-zone geometry may influence modern deformation.

Crustal Stress in the CEUS

The maximum horizontal compressive stress direction ($\sigma_{H\max}$) in the CEUS is broadly ENE–WSW (e.g., Sbar and Sykes, 1973) across thousands of kilometers (Fig. 1a). This long-wavelength

$\sigma_{H\,\max}$ parallels the ENE–WSW compressional traction applied by Mid-Atlantic Ridge push and the compression expected from absolute plate motion (via asthenospheric drag traction; e.g., Zoback and Zoback, 1980). These observations were taken as early evidence that plate tectonic processes control intraplate stress and have led to the conventional understanding that the stress field in the CEUS is more or less homogeneous, compressive, and driven by global tectonic processes (e.g., Zoback, 1992).

Horizontal principal stress directions in the ETSZ conform to the CEUS-wide pattern of ENE–WSW $\sigma_{H\,\max}$ (Fig. 1a). Five sets of borehole breakouts NNE and ESE of the ETSZ proper (compiled by Heidbach *et al.*, 2018) have an average $\sigma_{H\,\max}$ of N58°E (trends of near-horizontal axes are listed as N[mod(azimuth,180)]°E. When explicitly stated, fault orientations are [strike azimuth]/[dip angle]°, with dip down to the right when looking to the strike azimuth). Similarly, the 26 first-motion focal mechanisms of Chapman *et al.* (1997) are dominated by ENE–WSW maximal shortening axes (*P* axes); formal inversion of these mechanisms (Mazzotti and Townend, 2010) yields a best-fit $\sigma_{H\,\max}$ of N54°E. Because these unremarkable principal stress directions give no reason to question conventional understanding of a plate-scale tectonically driven stress field, ETSZ seismicity has mainly been interpreted as simple reactivation of inherited faults (e.g., Powell *et al.*, 1994; Chapman *et al.*, 1997; Mazzotti and Townend, 2010) by implication in a uniform stress field.

The most robust constraints on $\sigma_{H\,\max}$, especially in low-seismicity regions such as the CEUS, come from wellbore breakouts. These and other in situ indicators, however, typically contain little information outside of the horizontal plane and, therefore, do not demonstrate whether a region is undergoing net horizontal shortening, simple shear, or net horizontal extension (deformation styles typified by reverse, strike-slip, and normal faulting, respectively). By contrast, earthquake focal mechanisms directly record faulting style (Figs. 1a and 2a,b), albeit with weak constraint on stress directions (e.g., McKenzie, 1969). Consistent with the canon of ENE–WSW horizontal shortening parallel to, and inferred to result from, plate boundary and/or basal tractions, most CEUS earthquakes record reverse, reverse-oblique, or strike-slip motion (Fig. 2b) and have near-horizontal P axis that trend, on average, ENE–WSW (Fig. 1a).

Details of earlier studies, however, hint at an anomalous deformation style in the ETSZ (Figs. 1a and 2a,b). In contrast to the net horizontal shortening—reverse to oblique-reverse faulting—typical of CEUS focal mechanisms (Fig. 2b), negative rakes in 22 of 26 events studied by Chapman *et al.* (1997) and 18 of 26 studied by Cooley (2014) demonstrate a consistent component of net SE–NW extension.

Stress Inversions

The inversion of focal mechanisms for the normalized crustal stress tensor is well established and stems from the axiom that coseismic slip parallels the shear traction resolved on the fault plane (e.g., Angelier, 1979). The latter depends linearly on the orientation of the fault and on the 3D stress tensor; this linear system quickly becomes overdetermined with multiple slip observations from faults of different orientations. Inverting this system yields the normalized stress tensor that minimizes the angular misfit between the shear traction on the fault planes and the slip vectors.

The normalized stress tensor can be fully described in terms of the directions and relative magnitudes S of the three principal stresses. The stress ratio Φ is given as

$$\Phi = (S_2 - S_3)/(S_1 - S_3). \tag{1}$$

Simpson (1997) combined Φ with the style of faulting (normal, strike-slip, or reverse, as defined by principal axis plunges, Zoback, 1992) to describe the style of deformation as a quantity $A\Phi$:

$$A\Phi = (n + 0.5) + (-1)^n(\phi - 0.5), \tag{2}$$

with $n = 0$ for normal faulting, 1 for strike slip, and 2 for thrust. Consequently, $A\Phi$ defines a continuum from radial extension ($A\Phi = 0$) to radial contraction ($A\Phi = 3$), passing through uniaxial extension—pure normal faulting ($A\Phi = 0.5$), oblique extension ($A\Phi = 1.0$), horizontal shear–strike-slip ($A\Phi = 1.5$), oblique contraction ($A\Phi = 2.0$), and uniaxial contraction—pure reverse faulting ($A\Phi = 2.5$).

Thus, stress inversions (Fig. 2c,d) quantify the best-fitting deformation style ($A\Phi$) and principal stress directions. Variations in stress can be discussed in terms of differences in $A\Phi$ and $\sigma_{H\,\max}$. By contrast, most in situ stress indicators such as borehole breakouts are typically only meaningfully sensitive to $\sigma_{H\,\max}$.

Previous ETSZ stress inversions

At least three previous stress inversions have determined that the magnitudes of the NE–SW-trending $\sigma_{H\,\max}$ and vertical stress are approximately equal. As part of a study of 12 eastern North America seismic zones, Mazzotti and Townend (2010) inverted Chapman *et al.* (1997) 26 mechanisms, finding $\sigma_{H\,\max}$ N54°E ± 9° and $A\Phi \approx 1.2 \pm 0.25$ at 90% confidence (Mazzotti and Townend, 2010 do not list $A\Phi$ uncertainty, yet the confidence intervals for "S_1" and "S_2" plotted in their Fig. 2 overlap). Thus, they found no significant difference between the maximum (NE-SW, horizontal) and intermediate (vertical) stresses. Subsequently, Levandowski, Herrmann, *et al.* (2018) inverted those 26 solutions, four moment tensors from the ETSZ plus five from adjacent areas in western central Alabama (Herrmann, 2022; see Data and Resources), and 24 mechanisms derived by Cooley (2014), finding an extensional regime with substantial strike slip $A\Phi \approx 0.84 \pm 0.06$ (1 std). Most recently, Lund-Snee and Zoback (2020) used 19 of Chapman *et al.* (1997) mechanisms and three moment

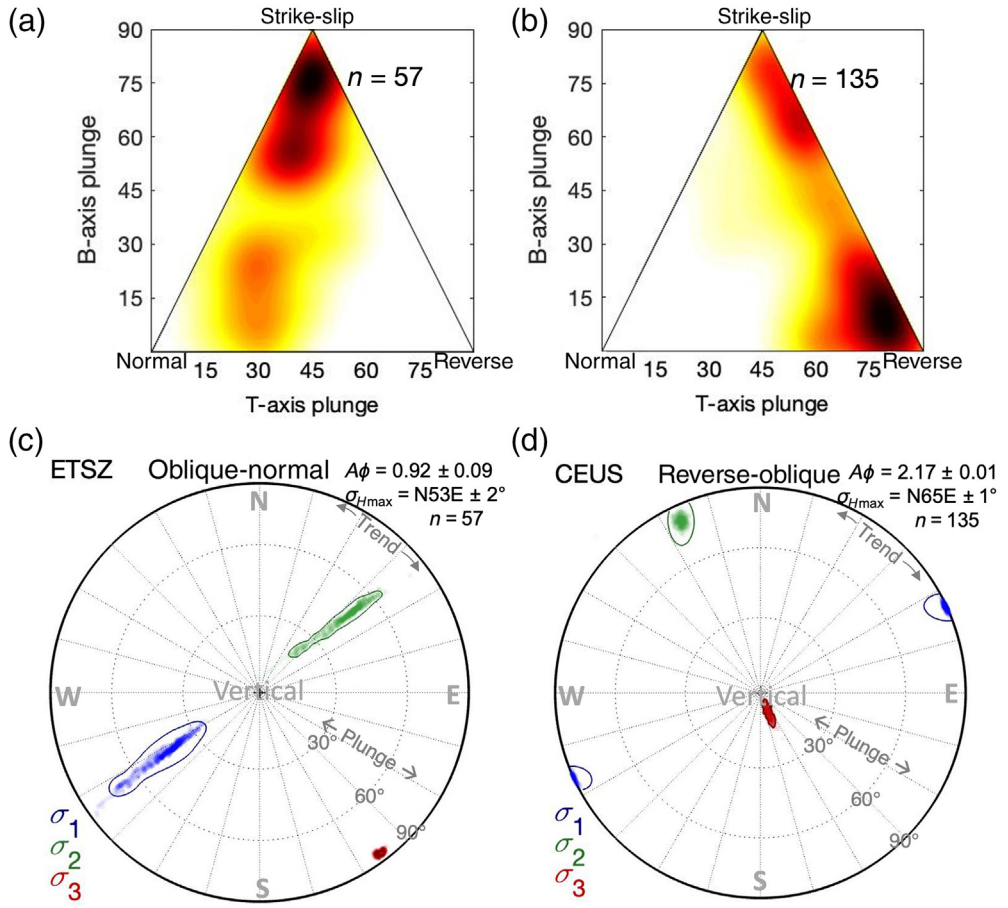

Figure 2. (a) Heat map of ETSZ faulting style classified by P/T/B axis plunges (following Frohlich and Apperson, 1992). (b) Heat map of central and eastern United States (CEUS) faulting style classified by P/T/B axis plunges (following Frohlich and Apperson, 1992) for the area shown in panel (b). Aftershocks of the 2011 M_w 5.65 Mineral, Virginia, event and seismicity in the New Madrid region are excluded for clarity and for reasons discussed in the supplemental material. (c) ETSZ stress inversion results (upper hemisphere projection) using geomechanically favorable solutions. The maximally compressive stress (σ^1) is near-vertical and insignificantly greater than the near-horizontal, N53E trending σ^2. Deformation comprises northwest (NW)–southeast (SE) lengthening, and both vertical and NE–SW shortening. (d) CEUS stress inversion results: deformation comprises N65E°-directed shortening and vertical lengthening dominated by reverse faulting. The color version of this figure is available only in the electronic edition.

tensors, resulting in $A\Phi = 1.32 \pm 0.11$ (1 std). All of these findings document significantly lower $A\Phi$ in the ETSZ than elsewhere in eastern North America.

The main data source(s) for these previous studies—first-motion focal mechanisms (Chapman *et al.*, 1997; Cooley, 2014)—are nonunique solution sets. In both the cases, FOCMEC (Snoke *et al.*, 1984) was used to determine an ensemble of strike/dip/rake combinations that reproduce polarities with the minimum number of errors. In some cases, more than 100 solutions were determined. This wealth of options notwithstanding, only one mechanism for each event was ultimately published. This "median" solution provided no better fit than other options but was chosen for having the median strike of the acceptable solution set. Here, we retain all minimum-mismatch solutions as a prior distribution of focal mechanisms for each event and conduct our inversions using this ensemble of possibilities. Doing so propagates uncertainties from first-motion polarities through the resultant stress tensor and allows us to leverage geomechanical constraints to generate a better informed posterior distribution.

Dataset and inversion details

We compile focal mechanisms for 57 earthquakes in the ETSZ proper (orange box in Fig. 1a). These include the full set of FOCMEC solutions for 25 events derived by Chapman *et al.* (1997) from *P*-wave first motions (one event outside of the ETSZ is excluded). We also generate new solution sets for 24 additional earthquakes using *P*- and *SH*-wave polarities plus amplitude ratios; Cooley (2014) originally examined many of these waveforms with *P* and *SH* polarities alone, so this analysis supersedes those results. The remaining eight events are constrained by moment tensors derived from waveform fitting (Herrmann, 2022; U.S. Geological Survey [USGS], 2022, see Data and Resources; Daniels and Peng, 2022).

This dataset differs from those used in the previous studies in a few ways. In addition to the 24 new solution sets we derived, five moment tensors from comparatively recent events have not been previously used in ETSZ stress inversions. These earthquakes include 2020 M_w 3.8 Fincastle, Tennessee, and the 2018 M_w 4.4 Decatur, Tennessee mainshock (Herrmann, 2022; USGS, 2022), and three other events from the Decatur sequence (Daniels and Peng, 2022). Second, Levandowski, Herrmann, *et al.* (2018) included five moment tensors from west-central Alabama and one from Perry County, Kentucky, in their ETSZ inversion. Because one of the goals of the present study is to determine whether these

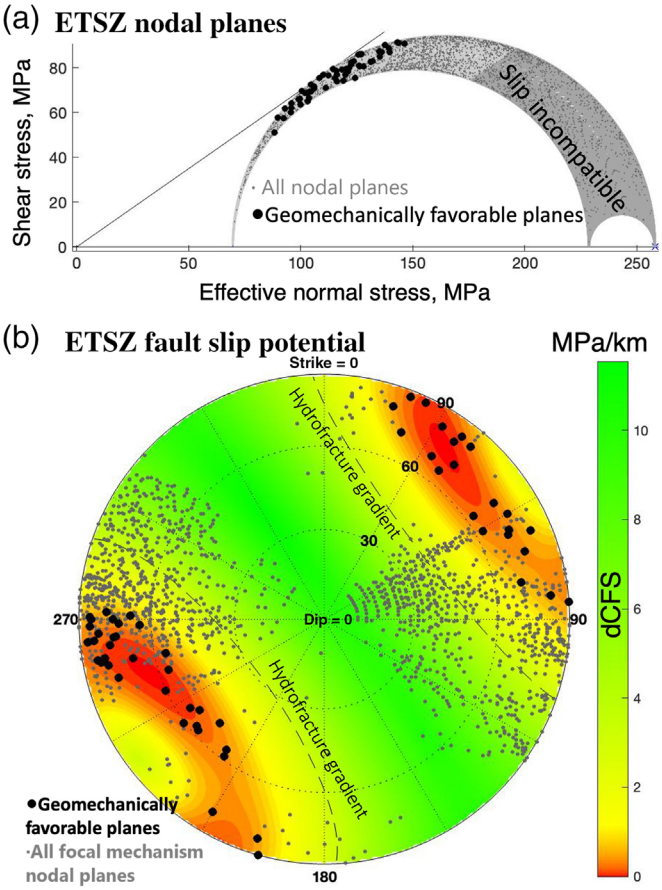

Figure 3. (a) Mohr circle of all ETSZ focal mechanism nodal planes (gray dots) and the most geomechanically favorable plane for each event (black dots). Many of the nodal planes that reproduce first-motion polarities are nonetheless incompatible with frictional slip. These planes are inadmissible to stress inversions. By contrast, all of the favorable planes are geomechanically viable. (b) Slip potential of ETSZ faults. Polar contour plot of dCFS as a function of fault orientation (dCFS = friction × |normal traction gradient| − |shear traction gradient|), which is the difference between the critical shear stress and the resolved shear stress. The dashed black lines indicate hydrofracture gradient or the limit of slip compatibility. The gray dots indicate the strike and dip of nodal planes from all ETSZ focal mechanisms. Notably, many are slip incompatible. The black circles indicate geomechanically favorable solution for each earthquake. All of these planes are compatible with slip. The color version of this figure is available only in the electronic edition.

outlying areas experience the same stress state as the ETSZ, we will defer analysis of these regions until after investigating the ETSZ proper. Third, we add six moment tensors from Greene County, Alabama (Chen and Wolf, 2018) to that dataset from surrounding areas considered later.

The most important methodological difference between this and the previous studies is that we consider the full ensemble of FOCMEC solutions for a given event. On average, 30 equally acceptable solutions are found for each event (Table S2, available in the supplemental material to this article, presents the full suite of focal mechanisms for each event). By contrast, only the "median" solution—the mechanism with the median strike among the accepted models—for each event was presented by Chapman *et al.* (1997) and Cooley (2014). All the previous studies (Mazzotti and Townend, 2010; Levandowski, Herrmann, *et al.*, 2018; Lund-Snee and Zoback, 2020) considered only this single pair of nodal planes for each event.

Nonuniqueness is inherent in stress inversions. The ambiguity between nodal planes, which is the focal and the auxiliary plane, is well known; the two are equally admissible with respect to first-motion polarities. Thus, Vavryčuk (2014) developed a formalism that randomly selects one of the two nodal planes of each mechanism and then iteratively inverts, computes the stability of both nodal planes in the derived stress field, and selects the less stable for each event. For the first-motion mechanisms considered here, we have not only two acceptable planes but an average of ∼60 for each event (∼30 mechanisms, each with two nodal planes). To capitalize on this range of admissible solutions, we generalize Vavryčuk (2014) geomechanical instability consideration. For each of 1000 realizations of the iterative inversion, an initial stress estimate is generated by randomly selecting one solution (which comprises two nodal plane options) for each event and following Vavryčuk's approach. Because friction influences instability, we assign a random friction 0.4–1.0 in each realization. From this initial estimate of the normalized stress tensor, we calculate the full stress tensor (following Walsh and Zoback, 2016; Levandowski, Weingarten, *et al.*, 2018, using a hydrostatic pore pressure gradient and a vertical stress gradient of 27 ± 2 MPa/km). The full stress tensor allows us to compute the shear and normal tractions on each plane being considered (Fig. 3a), and quantify instability in terms of distance from Coulomb failure (Fig. 3b), or the difference between the computed shear traction magnitude and the critical shear traction:

$$\mathrm{dCFS} = \mathrm{friction} \times |\mathrm{normal\ traction\ gradient}| - |\mathrm{shear\ traction\ gradient}|. \quad (3)$$

Notably, we find that many of the polarity-based nodal planes may be frictionally incompatible with slip; pore-fluid pressures greater than the minimum stress would be needed to reduce effective normal stress enough for slip to occur, so the rock would hydrofracture before hosting an earthquake (Fig. 3a). For some focal mechanisms, both the nodal planes may be incompatible. Each such inadmissible solution must be swapped for an alternative mechanism for the same event. This substitution is typically straightforward, because the poorly constrained events feature many strike/dip/rake combinations that account for the (sparse) polarity constraints.

One approach to this selection is to determine which alternatives are slip compatible and randomly select one, then move

on to the next iteration: invert, recompute the full stress tensor, and replace locked planes as necessary. Each of the 1000 realizations comprises 10 invert–select–replace–invert iterations, while holding the friction and lithostatic gradient constant. Results of these "slip compatible" inversions are presented in Figure S1. To further leverage geomechanical constraints on the nonunique focal mechanisms, however, we prefer a more restrictive approach that identifies and selects each event's least stable option (i.e., that with the lowest dCFS; Fig. 3b). The 57 "geomechanically favorable" mechanisms are then inverted to complete one iteration. Again, we complete 10 such iterations in each of 1000 realizations. Importantly, both the "slip compatible" and "geomechanically favorable" approaches identify frictionally acceptable mechanisms for each of the 57 earthquakes (Fig. 3a).

Results

Inversions of the geomechanically favorable planes (Fig. 2c) yield best-fit stress tensors with ENE–WSW $\sigma_{H\,\mathrm{max}}$ (N51°E ± 3°), which is both consistent with the general trend across the CEUS and with five sets of borehole breakouts near the ETSZ that average $\sigma_{H\,\mathrm{max}}$ N58°E (compiled by Heidbach *et al.*, 2018). Nevertheless, the inversions also give $A\Phi = 0.92 \pm 0.09$, meaning that $\sigma_{\mathrm{vertical}} \approx \sigma_{H\,\mathrm{max(NE–SW)}} \gg \sigma_{H\,\mathrm{min(NW–SE)}}$. The "slip compatible" inversion yields insignificantly higher $A\Phi = 1.03 \pm 0.12$ ($\sigma_{H\,\mathrm{max(NE–SW)}} \approx \sigma_{\mathrm{Vertical}} \gg \sigma_{H\,\mathrm{min(NW–SE)}}$). The oblique extensional deformation regime documented by either method is quite unlike any other major seismic zone in eastern North America.

The stress state does not appear to be depth-dependent. There is no significant difference between inversions of 29 ETSZ events shallower than 15 km and the 28 deeper events (Fig. S2). Similarly, ETSZ extension is not restricted to the NYAL bend. Inversions of 28 events east of and near the bend do yield somewhat lower $A\Phi$ (0.80 ± 0.06) than inversions of the 29 events away from the bend ($A\Phi = 0.97 \pm 0.13$), however (Fig. S3).

For comparison, we determine regional stress outside the ETSZ (Fig. 2d) using 135 mechanisms from the region shown in Figure 1b, which are mostly constrained by moment tensor inversions (Herrmann, 2022; USGS, 2022). These inversions quantify the known (e.g., Sbar and Sykes, 1973) reverse to reverse-oblique stress regime in the southeastern U.S. as $A\Phi = 2.17 \pm 0.01$; this result differs from the ETSZ state of stress by more than 13 standard deviations. Stress inversion results for broader regions of the CEUS, and inversions of subsets of the region are shown in Figure S4; all document reverse- to reverse-oblique faulting environments.

Discussion

Mechanical considerations

The performance of the geomechanically constrained stress inversions can be evaluated from two metrics of the individual constituent focal mechanisms—dCFS and angular misfit—that provide independent perspectives of the goodness of fit. On the one hand, dCFS is a function of only the strike and dip of the focal plane; whereas, on the other hand, angular misfit essentially depends on only the rake (for a given plane). Low dCFS implies internal consistency among the focal plane choices and consistency of the focal planes with the associated stress tensor, but this metric is corrupted by our use of dCFS as the criterion for focal plane selection in the "geomechanically favorable" inversions. The angular misfit between the slip vectors and resolved shear tractions is the quantity very minimized by the stress inversions; low misfits imply good fit and a locally homogenous stress field (e.g., Michael, 1991; Hardebeck, 2012), but do not guarantee that the selected mechanisms are geomechanically admissible (e.g., Fig. 3a). We suggest that considering the two quantities together sheds light on the internal consistency of each stress inversion (Fig. 4a). The median dCFS and misfit of the "geomechanically favorable" inversions are 0.28 MPa/km and 18° versus 1.78 MPa/km and 27° for the "slip compatible" inversions. Thus, our preferred approach performs better on both the metrics. Future work may wish to define an objective function that explicitly combines angular misfit and dCFS for use as the criterion for iterative focal versus nodal plane determination.

Geomechanical constraints on the spatial extent of anomalous ETSZ stress

Hundreds of data near New Madrid demonstrate a distinct state of stress and broadly bound the westward extent of the ETSZ to somewhere in central Tennessee (Fig. 3b). Similarly, thrust mechanisms (Fig. 1a) and stress inversions (Fig. S4) in South Carolina bound its southern and eastern sides. The oblique-reverse 2020 M_{w} 5.1 Sparta, northwestern North Carolina, earthquake (Figueiredo *et al.*, 2022) and a single oblique-reverse earthquake in southwestern North Carolina (Chapman *et al.*, 1997; their event 20) may delineate the eastern stress boundary to within ~100 and ~20 km, respectively. To the northwest, northeast, and southwest of the ETSZ, however, the extents of the anomalous ETSZ stress field have not been previously determined.

We will next examine single focal mechanisms from these surrounding areas, and quantify their dCFS and angular misfit in the ETSZ stress field (Fig. 3a). This approach allows us to compare the local state of stress in these surrounding areas with the ETSZ stress field, and it is useful in areas with insufficient data for stand-alone stress inversions (20–25 mechanisms are needed for reliable inversions, e.g., Townend and Zoback, 2001; Martínez-Garzón *et al.*, 2016).

For instance, Carpenter *et al.* (2014) note that the 2012 Perry County, Kentucky, earthquake—a strike-slip mechanism at 17 km depth with negative rakes on both nodal planes—resembles the deep, oblique-normal faulting characteristic of the ETSZ. They, therefore, suggest that the ETSZ extends at least this far—70 km or so north into Kentucky. To test this

idea, we compute the dCFS and angular misfit for their mechanism, two moment tensor solutions, and 102 of our own polarity-based solutions. Many of these options invoke well-suited focal planes that are both unstable in the ETSZ stress field and have slip vectors subparallel to the shear traction resolved on those planes. The best-fitting mechanism has dCFS 0.29 MPa/km and 9° misfit, implying that it is more compatible with the ETSZ stress tensor than (the median of) the ETSZ events used to determine that tensor. Thus, this mechanism is consistent with Carpenter *et al.* (2014) suggestion that the ETSZ stress field continues into southeastern Kentucky.

Having speculatively established that the ETSZ stress field reaches as far as southern Kentucky, we will next look 200 km farther NNW to the 1980 M_w 5.04 Mt. Sterling, Kentucky, earthquake. The less stable plane from Herrmann (2022) moment tensor solution—strike/dip of 030°/60°—is 0.8 MPa/km from failure, with an angular misfit of 51°. This comparatively poor fit leads us to speculate that the NNW extent of ETSZ stress field lies between southeastern and north-central Kentucky.

To determine whether the ETSZ stress field continues to the NE beyond southeastern Kentucky, we examine the Giles County seismic zone, Virginia, ~250 km ENE. Six *P*-polarity single-event focal mechanisms and five composite solutions (Munsey and Bollinger, 1985), and a solution for the 2017 m_b 3.9 earthquake derived from *P*-polarity, *SH*-polarity, and *SH*/*P* amplitude ratios (DePaolis and Chapman, 2018) are generally poorly fit by the ETSZ stress field (median dCFS 0.57 MPa/km, median misfit 40°). The northeastern edge of the ETSZ may, thus, be somewhere near the Virginia-Kentucky state border. As mentioned earlier, the oblique-reverse 2020 Sparta, North Carolina, earthquake and numerous thrust earthquakes in South Carolina are not compatible with the ETSZ stress field, consistent with this maximum eastward extent. The obvious differences between the ETSZ and New Madrid earthquakes constrain the westward limit of the ETSZ to generally in central Tennessee.

We can constrain the southwestern extent of ETSZ-style NW–SE oblique extension with 11 moment tensors from central and western Alabama, albeit speculatively, to within 30 or so kilometer in western Alabama. Closest to the ETSZ, three moment tensors (Herrmann, 2022) from central Alabama fit well with the ETSZ stress field in that they include planes that average 0.28 MPa/km from failure, and their slip averages 14° misfit from the resolved shear traction from the ETSZ stress tensor. Moreover, the faulting styles and principal axes—two normal and one strike slip with near-horizontal T axis averaging N133°E—resemble the dominant characteristics of ETSZ seismicity. The two main differences between these events and typical ETSZ earthquakes are their occurrence ~50 km west of the NYAL and somewhat shallower hypocenters (average 7.2 km, as deep as 12.7 km). We, thus, suggest that the ETSZ stress field may continue as far southwest as the most distal of these events, the 2004 M_w 4.2 Forkland, Alabama, earthquake in southernmost Greene County.

Ten years later and only 30–40 km north, in northwestern Greene County, a swarm-like cluster of seismicity availed eight moment tensors (Chen and Wolf, 2018; Herrmann, 2022). All the eight are strike-slip events on faults that are suitable for slip in the ETSZ stress field (average 0.35 MPa/km from failure), yet the slip directions differ substantially from the shear traction predicted on the fault planes, with an angular misfit of 36°. Specifically, there is an apparent rotation of the stress field that manifests in an average N85°E P axis trend, some 30° clockwise from that in the ETSZ. We speculate that these northwestern Greene County mechanisms may record the transition from ETSZ-type NW–SE extension to the strike-slip faulting with more easterly P axis that dominates Guy-Greenbrier (Arkansas), east Texas, and into central Oklahoma (Levandowski, Herrmann, *et al.*, 2018; Lund-Snee and Zoback, 2020).

In summary (Fig. 3b), our observations place speculative limits on the overall extent of the anomalous ETSZ stress field. Although it has been previously known that ETSZ extension does not affect areas to the east (e.g., in South Carolina) or west (e.g., New Madrid), here we find that the ETSZ stress field appears compatible with focal mechanisms as far northeast as southeastern Kentucky and as far southwest as west-central Alabama. The same geomechanical calculations suggest that the ETSZ stress field does not extend to northern Kentucky and does not branch west to Giles County, Virginia. Finally, we find that the anomalous NW–SE oblique extension characteristic of the ETSZ is stable with respect to depth (Fig. S2) and location within the seismic zone (e.g., east and west of the NYAL; Fig. S3).

Possible origins of anomalous stress

Of the three general explanations possible for elevated seismicity rates in the ETSZ, neither natural periodicity nor weak material readily explains the distinct state of stress. This absence of evidence does not imply that there is not a weak zone in the ETSZ or that instrumentally recorded earthquake rates represent a steady-state average; these factors could contribute to elevated modern seismicity rates, but they do not account for the anomalous stress field. A source of stress derived from something other than plate boundary or basal tractions, which sums in a tensor sense with the regional field, is the most straightforward explanation for the change in net stress.

This local stressor does not markedly alter horizontal principal stress directions, but instead perturbs the relative magnitude of the vertical stress. To the east of the ETSZ in South Carolina, ($A\Phi = 2.44$) $\sigma_{ENE-WSW} > \sigma_{SSE-NNW} > \sigma_{vertical}$, and to the north and west ($A\Phi = 1.87$) $\sigma_{ENE-WSW} > \sigma_{vertical} \gtrsim \sigma_{SSE-NNW}$. By contrast, $\sigma_{vertical} \gtrsim \sigma_{ENE-WSW} \gg \sigma_{SSE-NNW}$ in the ETSZ. Thus, the anomalous stress increases vertical compression, decreases both horizontal stress components, or increases vertical and decreases one or both horizontal stresses. Changing surface loads, flexural

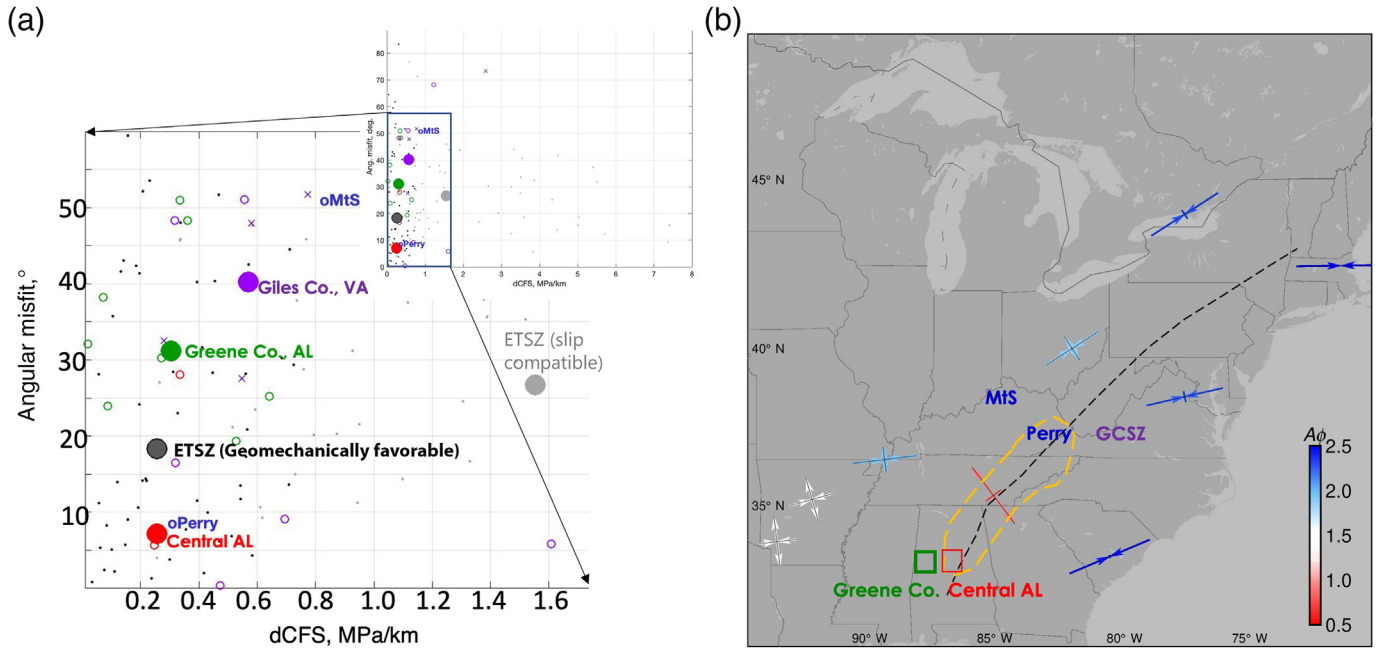

Figure 4. (a) Consistency of focal mechanisms with the ETSZ stress field. For the ETSZ inversions, the median dCFS and angular misfit are significantly lower for the "geomechanically favorable" inversion (large black circle) than the "slip compatible" inversion (large gray dot). The misfit and dCFS for the individual focal mechanisms are shown as small black and gray dots. Both the 2012 Perry County, Kentucky (blue "Perry") and central Alabama earthquakes (median indicated by red circle and individual events indicated by red dots) exhibit similar dCFS and lower angular misfit than even the favorable ETSZ solutions. The ETSZ stress field likely encompasses these areas. By contrast, Mt. Sterling, Giles County, and Greene County mechanisms are not well fit by the ETSZ stress field, providing limits on its spatial extent. (b) Possible extent of the ETSZ stress field indicates the deformation trajectories determined from stress inversions (arrows) colored by $A\Phi$. Outward arrows denote horizontal extension. Inward arrows denote shortening. For example, strike-slip faulting near Guy-Greenbrier, AR, ($A\Phi = 1.53$) corresponds to nearly equal parts east-northeast (ENE)–west-southwest (WSW) shortening and north-northwest (NNW)–south-southeast (SSE) lengthening. By contrast, thrust faulting ($A\Phi \approx 2.50$) along the eastern margin represents ENE–WSW shortening and vertical extension with no substantial horizontal lengthening perpendicular to $\sigma_{H\max}$. Oblique NW–SE extension spans from central Alabama, through the ETSZ, to southeastern Kentucky. Its overall extent is bounded (clockwise from north) by the Mt. Sterling event (MtS), Giles County (GCSZ), South Carolina, Greene County, and New Madrid. The location of the ETSZ-like Perry County, KY, earthquake is also indicated. The color version of this figure is available only in the electronic edition.

stress, and gravity-derived stress, all of which co-occur with isostatic disequilibrium, are possible sources of the perturbed stress state. Furthermore, the negative isostatic residual gravity implies isostatic overcompensation or mass deficit relative to surface elevation; absent flexural strength and, in steady state, the ETSZ would be at a higher elevation than at present.

A very similar situation has been described in two other Proterozoic plate-boundary Proterozoic suture zones also now located in intraplate North America, the Yavapai-Mazatzal suture in Colorado, and the Yavapai–Wyoming Craton suture or "Cheyenne belt" in Wyoming (western Great Plains, United States). Uncompensated low-density lower crust generates suture-normal tension and extension in the overlying crust, and preferential flux of fluids from the dewatering Farallon slab along lithospheric-scale fractures (i.e., sutures) and resultant hydration-induced retrogression of garnet-bearing lower crustal assemblages was offered as a possible explanation for that low-density lower crust (Levandowski *et al.*, 2017). In addition to the similarities in Paleo-Plate Boundary tectonic setting between the NYAL and the western sutures, magnetotelluric evidence (Murphy and Egbert, 2017) suggests cold but hydrated uppermost mantle lithosphere beneath the southern Appalachians—an interpretation also consistent with *Pn* tomography (MacDougall *et al.*, 2015). This hydration may furthermore play a part in a positive feedback with small-scale convection that has been suggested as responsible for Miocene topographic rejuvenation in the southern Appalachians (Liu, 2014). Time-dependent topography can focus seismicity (Becker *et al.*, 2015) as the brittle crust adjusts to changing buoyancy and flow in the underlying upper mantle.

The stress perturbation associated with the western shear zones, however, occurs in a low regional-stress setting, effectively farther from plate-boundary compressive tractions, in which ambient deformation is mostly extensional and extension directions vary. As such, gravity-derived stress is the dominant source of deviatoric stress (Flesch *et al.*, 2000; Levandowski *et al.*, 2017). In the ETSZ, however, the regional

contractional deformation field is overprinted, and plate tectonic compression is locally overcome. Furthermore, topographic rejuvenation is observed elsewhere in the southern Appalachians (e.g, Liu, 2014), including many seismically quiescent regions. Therefore, the presence of an inherited suture, and any related geodynamic process, is insufficient to account for focusing modern seismicity in the ETSZ.

The unique structure of the ETSZ inherited from Proterozoic shear geometry may further influence the interplay between upper mantle processes and seismicity. Crustal-scale concentrated deformation manifests, for example, in low-velocity crust from the near surface to midcrust or deeper (Powell *et al.*, 2014). This damage zone may provide an efficient set of conduits for mantle-derived fluids; indeed, lower crustal serpentinization or other modification has been suggested to explain the absence of a distinct Moho arrival on receiver functions near the kink in the NYAL (Graw *et al.*, 2015). The density-decreasing effects of hydration can be most profound in low-temperature lower crust that is firmly in the garnet stability field, in which hydration can induce retrogression of garnet-bearing assemblages to amphiboles and micas (Jones *et al.*, 2015; Butcher *et al.*, 2017). Therefore, the availability of pathways via suture zones between adjacent distinct terranes and/or through heavily fractured crust, especially if these inherited fractures now are in a state of deviatoric tension, may control the degree and lateral extent of buoyancy increase due to hydration (e.g., Levandowski, Jones, *et al.*, 2018), and therefore the associated (tensile) stress increase.

These speculated bottom-up effects would be symbiotic with documented anomalous surface processes in the ETSZ. A late-Miocene base-level drop of ∼150 m in the Tennessee River basin triggered the rapid erosion of Paleozoic sedimentary units from an ∼70 km by 350 km swath (WNW–ESE by NNE–SSW; Gallen and Thigpen, 2018). This unloading has a functionally identical effect to increased subseismogenic zone buoyancy: The overlying material tends to increase in elevation and in so doing is put in relative horizontal tension parallel to the short axis of the eroded swath (i.e., in a WNW–ESE direction). Although our speculated areal extent of the ETSZ stress field extends hundreds of kilometer farther SW and NE than the region of documented rapid erosion, the densest ETSZ seismicity is ringed by geomorphic knickpoints that are testaments to the time dependence of topography in the region, and quantitative estimates of total long-term stress perturbations based on the volume of eroded material reach a few MPa (Gallen and Thigpen, 2018). Therefore, a feedback between crustal, lithospheric, or deeper buoyancy and surficial processes may further focus ETSZ earthquakes.

Favorable faults and limitations on ETSZ seismicity

Geomechanically favorable fault orientations in the ETSZ (e.g., red areas in Fig. 2b) are restricted to strikes in the NE and SW quadrants and dips 50° or steeper. The most susceptible planes form two continua in strike/dip/style: one from 015°/90°/strike slip to 055°/60°/normal to 090°/90°/strike slip and one approximately diametric. Across 1001 inversions seeded with different focal plane choices, using friction anywhere from 0.4 to 1.0, and 69 events spanning the greater ETSZ—west-central Alabama to southeastern Kentucky—only strikes 013°–093° or 192°–275°, and dips $\gtrsim$ 50° are ever ultimately selected. In fact, faults striking 115°–175° or 295°–355° and all faults dipping less than ∼35° may lie beyond the hydrofracture gradient, and thus be geomechanically incompatible with slip.

These observations imply that paleoseismic investigations in the ETSZ, which are challenged by steep topography, active surface processes, and dense vegetation, may benefit from focusing on NNE–SSW or E–W-trending lineaments or NE–SW-trending scarps. By contrast, features trending north–south may not be fruitful. Quaternary near-surface or surface faulting has been suggested at three locations in the ETSZ (Hatcher *et al.*, 2012; Warrell *et al.*, 2017; Cox *et al.*, 2022) and all feature NE-striking primary faults. Near Douglas Lake (site DL-6 of earlier studies), a N55°E/30° thrust fault displaces Quaternary material and flattens down-dip to less than 15°; researchers have speculated that a trend of fissures extends SW below the lake for ∼1.5 km to join with observed collinear fissures (site DL-9) that they argue may have formed above a blind portion of the same thrust since ∼15.7 ka. Near Alcoa, Tennessee, a N60°E/41° thrust exposed along the Little River offsets ∼10.4 ± 1 ka alluvium (Cox *et al.*, 2022). Finally, near Vonore, Tennessee, a N57°E/77° thrust in 135 ± 1 ka gravels and a N42°E/58° normal fault in 31 ± 2 ka gravels 2.4 km southwest along Tellico Lake were observed (Cox *et al.*, 2022).

Although only the latter of these four proposed Quaternary faulting events may appear consistent with the stress field at seismogenic depths (>5 km, on average ∼15 km) in the ETSZ, near-surface deformation patterns often differ from hypocentral motions. Such a phenomenon was directly observed in the 2020 M_w 5.1 Sparta, North Carolina, earthquake; the surface rupture—the first ever documented in the eastern U.S.—chiefly comprised dip-slip on low-angle, NE-vergent reverse faults (Figueiredo *et al.*, 2022), whereas hypocentral motion (Herrmann, 2022; USGS, 2022) and permanent displacements of local geodetic monuments record dominantly sinistral motion with a secondary reverse component. Therefore, it is unlikely that the four paleoseimological observations represent surface ruptures along the mainshock fault planes, but they certainly may record hanging wall contraction above NE/SW-trending basement normal faults or NNE/SSE- to E/W-trending oblique faults. The decollement between overthrust, allochthonous Paleozoic units and the Grenville-aged crystalline basement may accommodate such a disconnect. Alternatively, these Pleistocene displacements could result from deglacial adjustments at the southern margin of the forebulge.

Conclusions

Stress inversions document an oblique extension in the ETSZ that is unique in the CEUS. Although stress inversions alone cannot uniquely identify the cause of elevated ETSZ earthquake rates, they do point to a distinct state of stress and therefore distinct long-term deformation within the ETSZ. We suggest that the spatial extent of anomalous stress outlines the footprint of the phenomena responsible for concentrated seismicity. The ETSZ as a stress province may extend northeastward into southeastern Kentucky, as suggested by Carpenter *et al.* (2014), and might continue more than 200 km farther southwest than generally understood, to west-central Alabama. By contrast, the Giles County seismic zone, Virginia, does not appear to record the same stress state as the ETSZ.

The uniqueness of the ETSZ bears implications for seismic hazard. It stands to reason that distinct stress implies a distinct strain regime, both in terms of the mode of deformation here, because oblique extension amid a continent undergoing net horizontal shortening, and earthquake rates. The footprint of this distinct seismotectonic setting may be the best available proxy for the area of elevated long-term seismic hazard associated with the ETSZ.

Data and Resources

The supplemental information contains the complete sets of focal mechanism solutions for each event, the most geomechanically favorable solution for each event, and additional stress inversions. Waveforms are available from the Incorporated Research Institutions for Seismology (IRIS) Data Management Center available at https://www.iris.edu (last accessed May 2022). Moment tensors were provided by St. Louis University North America Moment Tensor Catalog available at https://www.eas.slu.edu/eqc/eqc_mt/MECH.NA/MECHFIG/mech.html (last accessed November 2022) and U.S. Geological Survey (USGS) available at https://earthquake.usgs.gov/earthquakes/search/ (last accessed November 2022). Moment tensors for Greene County, Alabama, earthquakes were provided by Jian Chen and Lorraine Wolf. The complete solution sets for the focal mechanisms derived for this study are listed in Table S2. MATLAB codes for stress inversions, full tensor calculations, and slip potential modeling are available at https://github.com/WillLevandowski/StressInversions (last accessed March 2023) and https://github.com/WillLevandowski/FaultSlipPotential (last accessed March 2023).

Declaration of Competing Interests

The authors acknowledge that there are no conflicts of interest recorded.

Acknowledgments

Partial funding was provided to W.L. by U.S. Geological Survey (USGS) Earthquake Hazards Program (EHP) Award Number G19AP00024. Jian Chen and Lorraine Wolf provided moment tensors for Greene County, Alabama, earthquakes.

References

Angelier, J. (1979). Determination of the mean principal directions of stresses for a given fault population, *Tectonophysics* **56,** T17–T26.

Becker, T. W., A. R. Lowry, C. Faccenna, B. Schmandt, A. Borsa, and C. Yu (2015). Western US intermountain seismicity caused by changes in upper mantle flow, *Nature* **524,** no. 7566, 458–461.

Biryol, C. B., L. S. Wagner, K. M. Fischer, and R. B. Hawman (2016). Relationship between observed upper mantle structures and recent tectonic activity across the southeastern United States, *J. Geophys. Res.* **121,** no. 5, 3393–3414.

Blackwell, D., M. Richards, Z. Frone, J. Batir, A. Ruzo, R. Dingwall, and M. Williams (2011). Temperature at depth maps for the conterminous US and geothermal resource estimates, *Geothermal Resources Council 2011 Annual Meeting*, Vol. 35, San Diego, California, 24–27 October 2011.

Bockholt, B. (2015). A seismogenic study of the central and eastern United States, *Doctoral Dissertation*, University of Memphis, Memphis, Tennessee, 173 pp.

Bockholt, B. M., C. A. Langston, and M. Withers (2015). Local magnitude and anomalous amplitude distance decay in the eastern Tennessee seismic zone, *Seismol. Res. Lett.* **86,** no. 3, 1040–1050.

Brandmayr, E., and G. Vlahovic (2016). The upper crust of the eastern Tennessee seismic zone: Insights from potential fields inversion, *Tectonophysics* **685,** 1–7.

Brandmayr, E., A. P. Kuponiyi, P. Arroucau, and G. Vlahovic (2016). Group velocity tomography of the upper crust in the eastern Tennessee seismic zone from ambient noise data, *Tectonophysics* **688,** 148–156.

Butcher, L. A., K. H. Mahan, and J. M. Allaz (2017). Late Cretaceous crustal hydration in the Colorado plateau, USA, from xenolith petrology and monazite geochronology, *Lithosphere* **9,** no. 4, 561–578, doi: 10.1130/L583.1.

Boyd, O. S., D. E. McNamara, S. Hartzell, and G. Choy (2017). Influence of lithostatic stress on earthquake stress drops in North America, *Bull. Seismol. Soc. Am.* **107,** no. 2, 856–868.

Calais, E., A. M. Freed, R. Van Arsdale, and S. Stein (2010). Triggering of New Madrid seismicity by late-Pleistocene erosion, *Nature* **466,** no. 7306, 608–611, doi: 10.1038/nature09258.

Carpenter, N. S., E. W. Woolery, and Z. Wang (2014). The M w 4.2 Perry County, Kentucky, earthquake of 10 November 2012: Evidence of the eastern Tennessee seismic zone in southeastern Kentucky, *Seismol. Res. Lett.* **85,** no. 4, 931–939.

Chapman, M. C., C. A. Powell, G. Vlahovic, and M. S. Sibol (1997). A statistical analysis of earthquake focal mechanisms and epicenter locations in the eastern Tennessee seismic zone, *Bull. Seismol. Soc. Am.* **87,** 1522–1536.

Chen, J., and L. W. Wolf (2018). A notable earthquake swarm in Alabama: Natural or anthropogenic? *Seismol. Res. Lett.* **89,** no. 4, 1583–1594.

Clark, D., A. McPherson, and R. Van Dissen (2012). Long-term behaviour of Australian stable continental region (SCR) faults, *Tectonophysics* **566,** 1–30, doi: 10.1016/j.tecto.2012.07.004.

Cooley, M. T. (2014). New set of focal mechanisms and geodynamic model for the eastern Tennessee seismic zone, *Master's Thesis*, University of Memphis.

Cox, R. T., R. D. Hatcher, S. L. Forman, R. Counts, J. Vaughn, E. Gamble, J. Glasbrenner, K. Warrell, N. Adhikari, and S. Pinardi (2022). Synthesis of recent paleoseismic research on quaternary faulting in the eastern Tennessee seismic zone, eastern North America: Implications for seismic hazard and intraplate seismicity, *Bull. Seismol. Soc. Am.* **112,** no. 2, 1161–1189.

D'Agrella-Filho, M. S., E. Tohver, J. O. S. Santos, S.-A. Elming, R. I. F. Trindade, I. I. G. Pacca, and M. C. Geraldes (2008). Direct dating of paleomagnetic results from Precambrian sediments in the Amazon craton: Evidence for Grenvillian emplacement of exotic crust in SE Appalachians of North America, *Earth Planet. Sci. Lett.* **267,** nos. 1/2, 188–199.

Daniels, C., and Z. Peng (2022). Fault orientation and relocated seismicity associated with the 12 December 2018 M w 4.4 Decatur, Tennessee, earthquake sequence, *Seismol. Soc. Am.* **93,** no. 6, 3454–3467.

DePaolis, J., and M. C. Chapman (2018). The mb(Lg) 3.9, September 13, 2017 earthquake on the Virginia—West Virginia border: A significant shock in the Giles county seismic zone, *Seismological Society of America Annual Meeting*, doi: 10.1785/0220180082.

Ebel, J. E. (2008). The importance of small earthquakes, *Seismol. Res. Lett.* **79,** no. 4, 491–493

Ebel, J. E., K. P. Bonjer, and M. C. Oncescu (2000). Paleoseismicity: Seismicity evidence for past large earthquakes, *Seismol. Res. Lett.* **71,** no. 2, 283–294.

Figueiredo, P. M., J. S. Hill, A. J. Merschat, C. M. Scheip, K. G. Stewart, L. A. Owen, R. Wooten, M. Carter, E. Szymanski, S. Horton, *et al.* (2022). The Mw 5.1, 9 August 2020, Sparta earthquake, North Carolina: The first documented seismic surface rupture in the eastern United States, *GSA Today* **32,** 4–11.

Flesch, L. M., W. E. Holt, A. J. Haines, and B. Shen-Tu (2000). Dynamics of the Pacific-North American plate boundary in the western United States, *Science* **287,** no. 5454, 834–836.

Frohlich, C., and K. D. Apperson (1992). Earthquake focal mechanisms, moment tensors, and the consistency of seismic activity near plate boundaries, *Tectonics* **11,** 279–296.

Gallen, S. F., and J. R. Thigpen (2018). Lithologic controls on focused erosion and intraplate earthquakes in the eastern Tennessee seismic zone, *Geophys. Res. Lett.* **45,** no. 18, 9569–9578, doi: 10.1029/2018GL079157.

Graw, J. H., C. A. Powell, and C. A. Langston (2015). Crustal and upper mantle velocity structure in the vicinity of the eastern Tennessee seismic zone based upon radial P-wave transfer functions, *J. Geophys. Res.* **120,** 243–258.

Hardebeck, J. L. (2012). Coseismic and postseismic stress rotations due to great subduction zone earthquakes, *Geophys. Res. Lett.* **39,** no. 21, doi: 10.1029/2012GL053438.

Hatcher, R. D., Jr, J. D. Vaughn, and S. F. Obermeier (2012). Large earthquake paleoseismology in the east Tennessee seismic zone: Results of an 18-month pilot study, in *Recent Advances in North American Paleoseismology and Neotectonics East of the Rockies*, Special Paper 493, R. T. Cox, M. P. Tuttle, O. S. Boyd, and J. Locat (Editors), Geological Society of America, Boulder, Colorado, 111–142.

Heidbach, O., M. Rajabi, X. Cui, K. Fuchs, B. Müller, J. Reinecker, K. Reiter, M. Tingay, F. Wenzel, F. Xie, *et al.* (2018). The World Stress Map database release 2016: Crustal stress pattern across scales, *Tectonophysics* **744,** 484–498

Herrmann, R. B. (2022). SLU North America moment tensor catalog, available at https://www.eas.slu.edu/eqc/eqc_mt/MECH.NA/MECHFIG/mech.html (last accessed 13 November 2022).

Johnston, A. C., and R. L. Kanter (1990). Earthquakes in stable continental crust, *Sci. Am.* **262,** 68–75.

Jones, C. H., K. H. Mahan, L. A. Butcher, W. B. Levandowski, and G. L. Farmer (2015). Continental uplift through crustal hydration, *Geology* **43,** no. 4, 355–358.

King, E. R., and I. Zietz (1978). The New York-Alabama lineament: Geophysical evidence for a major crustal crustal break in the basement beneath the Appalachian basin, *Geology* **6,** 312–318.

Levandowski, W., and C. A. Powell (2018). Evidence for strain accrual in the eastern Tennessee seismic zone from earthquake statistics, *Seismol. Res. Lett.* **90,** no. 1, 446–451, doi: 10.1785/0220180052.

Levandowski, W., R. B. Herrmann, R. Briggs, O. Boyd, and R. Gold (2018). An updated stress map of the continental United States reveals heterogeneous intraplate stress, *Nature Geosci.* **11,** 433–437, doi: 10.1038/s41561-018-0120-x.

Levandowski, W., C. H. Jones, L. A. Butcher, and K. H. Mahan (2018). Lithospheric density models reveal evidence for Cenozoic uplift of the Colorado plateau and Great plains by lower-crustal hydration, *Geosphere* **14,** no. 3, 1150–1164.

Levandowski, W., M. Weingarten, and R. Walsh III (2018). Geomechanical sensitivities of injection-induced earthquakes, *Geophys. Res. Lett.* **45,** no. 17, 8958–8965.

Levandowski, W., M. Zellman, and R. Briggs (2017). Gravitational body forces focus North American intraplate earthquakes, *Nat. Commun.* **8,** doi: 10.1038/ncomms14314.

Liu, L. (2014). Rejuvenation of Appalachian topography caused by subsidence-induced differential erosion, *Nature Geosci.* **7,** no. 7, 518–523.

Long, M. D., K. G. Jackson, and J. F. McNamara (2016). SKS splitting beneath transportable array stations in eastern North America and the signature of past lithospheric deformation, *Geochem. Geophys. Geosys.* **17,** no. 1, 2–15.

Lund-Snee, J.-E., and M. D. Zoback (2020). Multiscale variations of the crustal stress field throughout North America, *Nat. Commun.* **11,** doi: 10.1038/s41467-020-15841-5.

MacDougall, J. G., K. M. Fischer, D. W. Forsyth, R. B. Hawman, and L. S. Wagner (2015). Shallow mantle velocities beneath the southern Appalachians from Pn phases, *Geophys. Res. Lett.* **42,** no. 2, 339–345.

Martínez-Garzón, P., Y. Ben-Zion, N. Abolfathian, G. Kwiatek, and M. Bohnhoff (2016). A refined methodology for stress inversions of earthquake focal mechanisms, *J. Geophys. Res.* **121,** no. 12, 8666–8687.

Mazzotti, S., and J. Townend (2010). State of stress in central and eastern North American seismic zones, *Lithosphere* **2,** no. 2, 76–83, doi: 10.1130/L65.1.

McKenzie, D. P. (1969). The relation between fault plane solutions for earthquakes and the directions of the principal stresses, *Bull. Seismol. Soc. Am.* **59,** no. 2, 591–601.

Michael, A. J. (1991). Spatial variations in stress within the 1987 Whittier Narrows, California, aftershock sequence: New techniques and results, *J. Geophys. Res.* **96,** no. B4, 6303–6319, doi: 10.1029/91JB00195.

Munsey, J. W., and G. A. Bollinger (1985). Focal mechanism analyses for Virginia earthquakes (1978-1984), *Bull. Seismol. Soc. Am.* **75,** no. 6, 1613–1636.

Murphy, B. S., and G. D. Egbert (2017). Electrical conductivity structure of southeastern North America: Implications for lithospheric architecture and Appalachian topographic rejuvenation, *Earth Planet. Sci. Lett.* **462,** 66–75.

Murphy, B. S., L. Liu, and G. D. Egbert (2019). Insights into intraplate stresses and geomorphology in the southeastern United States, *Geophys. Res. Lett.* **46,** no. 15, 8711–8720.

Petersen, M. D., A. D. Frankel, S. C. Harmsen, C. S. Mueller, K. M. Haller, R. L. Wheeler, R. L. Wesson, Y. Zeng, O. S. Boyd, D. M. Perkins, *et al.* (2014). Documentation for the 2014 update of the United States National seismic hazard maps, *U.S. Geol. Surv. Open-File Rept. 2014-1091*, doi: 10.3133/ofr20141091.

Pollitz, F. F., and W. D. Mooney (2016). Seismic velocity structure of the crust and shallow mantle of the central and eastern United States by seismic surface-wave imaging, *Geophys. Res. Lett.* **43,** no. 1, 118–126.

Powell, C. A., and W. A. Thomas (2016). Grenville basement structure associated with the eastern Tennessee seismic zone, southeastern USA, *Geology* **44,** 39–42, doi: 10.1130/G37269.1.

Powell, C. A., G. A. Bollinger, M. C. Chapman, M. S. Sibol, A. C. Johnston, and R. L. Wheeler (1994). A seismotectonic model for the 300-kilometer-long eastern Tennessee seismic zone, *Science* **264,** 686–689.

Powell, C. A., M. M. Withers, R. T. Cox, G. Vlahovic, and P. Arroucau (2014). Crustal velocity structure associated with the eastern Tennessee seismic zone: Vp and Vs images based upon local earthquake tomography, *J. Geophys. Res.* **119,** no. 1, 464–489, doi: 10.1002/2013JB010433.

Ravat, D. N., L. W. Braile, and W. J. Hinze (1987). Earthquakes and plutons in the midcontinent-Evidence from the Bloomfield pluton, New Madrid rift complex, *Seismol. Res. Lett.* **58,** no. 2, 41–52.

Sbar, M. L., and L. R. Sykes (1973). Contemporary compressive stress and seismicity in eastern North America: An example of intraplate tectonics, *Geol. Soc. Am. Bull.* **84,** no. 6, 1861–1882.

Shen, W., and M. H. Ritzwoller (2016). Crustal and uppermost mantle structure beneath the United States, *J. Geophys. Res.* **121,** no. 6, 4306–4342.

Simpson, R. W. (1997). Quantifying Anderson's fault types, *J. Geophys. Res.* **102,** no. B8, 17909–17919.

Snoke, J. A., J. W. Munsey, A. G. Teague, and G. A. Bollinger (1984). A program for focal mechanism determination by combined use of polarity and SV-P amplitude ratio data, *Earthq. Notes* **55,** 15.

Stein, S., and M. Liu (2009). Long aftershock sequences within continents and implications for earthquake hazard assessment, *Nature* **462,** 87–89.

Steltenpohl, M. G., I. Zietz, J. W. Horton, and D. L. Daniels (2010). New York–Alabama lineament: A buried right-slip fault bordering the Appalachians and mid-continent North America, *Geology* **38,** 571–574, doi: 10.1130/G30978.1.

Thomas, W. A., and C. A. Powell (2017). Necessary conditions for intraplate seismic zones in North America, *Tectonics* **36,** no. 12, 2903–2917.

Townend, J., and M. Zoback (2001). Implications of earthquake focal mechanisms for the frictional strength of the San Andreas fault system, *Geol. Soc. Lond. Spec. Publ.* **186,** 13–21, doi: 10.1144/GSL.SP.2001.186.01.02.

U.S. Geological Survey (USGS) (2022). Search earthquake catalog, available at https://earthquake.usgs.gov/earthquakes/search/ (last accessed November 2022).

Vavryčuk, V. (2014). Iterative joint inversion for stress and fault orientations from focal mechanisms, *Geophys. J. Int.* **199,** no. 1, 69–77, doi: 10.1093/gji/ggu224.

Wagner, L. S., M. D. Long, M. D. Johnston, and M. H. Benoit (2012). Lithospheric and asthenospheric contributions to shear-wave splitting observations in the southeastern United States, *Earth Planet. Sci. Lett.* **341,** 128–138.

Walsh, F. R., III, and M. D. Zoback (2016). Probabilistic assessment of potential fault slip related to injection-induced earthquakes: Application to north-central Oklahoma, USA, *Geology* **44,** no. 12, 991–994.

Warrell, K. F., R. T. Cox, R. D. Hatcher, J. D. Vaughn, and R. Counts (2017). Paleoseismic evidence for multiple Mw ≥ 6 earthquakes in the eastern Tennessee seismic zone during the late quaternary, *Bull. Seismol. Soc. Am.* **107,** no. 4, 1610–1624, doi: 10.1785/0120160161.

Wesson, R. L., and O. S. Boyd (2007). Stress before and after the 2002 Denali fault earthquake, *Geophys. Res. Lett.* **34,** no. 7, doi: 10.1029/2007GL029189.

Zoback, M. L. (1992). Stress field constraints on intraplate seismicity in eastern North America, *J. Geophys. Res.* **97,** no. B8, 11,761–11,782.

Zoback, M. L., and M. Zoback (1980). State of stress in the conterminous United States, *J. Geophys. Res.* **85,** no. B11, 6113–6156, doi: 10.1029/JB085iB11p06113.

Manuscript received 22 November 2022
Published online 16 March 2023